An experimental and theoretical investigation of the effect of second-phase particles on grain growth during the annealing of hot-rolled AZ61 magnesium alloy

Mohseni, M.; Eivani, A. R.; Vafaeenezhad, H.; Jafarian, H. R.; Salehi, M. T.; Zhou, J.

DOI
10.1016/j.jmrt.2021.09.049

Publication date
2021

Document Version
Final published version

Published in
Journal of Materials Research and Technology

Available online at www.sciencedirect.com

jmr&t
Journal of Materials Research and Technology

journal homepage: www.elsevier.com/locate/jmrt

Original Article

An experimental and theoretical investigation of the effect of second-phase particles on grain growth during the annealing of hot-rolled AZ61 magnesium alloy

M. Mohseni [a], A.R. Eivani [a,*], H. Vafaeenezhad [a], H.R. Jafarian [a], M.T. Salehi [a], J. Zhou [b]

[a] School of Metallurgy and Materials Engineering, Iran University of Science and Technology, Tehran, Iran
[b] Department of Biomechanical Engineering, Delft University of Technology, Mekelweg 2, Delft, 2628 CD, the Netherlands

ARTICLE INFO

Article history:
Received 21 July 2021
Accepted 11 September 2021
Available online 28 September 2021

Keywords:
Magnesium
Hot rolling
Annealing
Recrystallization
Grain growth
Monte Carlo
Analytical model

ABSTRACT

The mechanical properties of a magnesium alloy strongly depend on its grain structure. It is desirable to minimize grain growth during the post-forming annealing treatment, thereby minimizing the loss in strength while regaining ductility. In the present research, the annealing of the hot-rolled AZ61 Mg alloy at different temperatures for different times was performed to reveal the kinetics of grain growth, as affected by the precipitation or dissolution of second-phase particles. Three approaches, i.e., experimental, analytical modeling and atomistic simulation were taken and the results were compared. The predictions made from the analytical model and Monte Carlo simulation were both in acceptable agreement with experimental results in terms of the resultant grain sizes. However, the Monte Carlo simulation showed advantages over the analytical model. It was found that with increasing annealing temperature and holding time, the fraction of second-phase particles reduced, which strongly affected the kinetics of grain growth, limiting grain size and grain size homogeneity. The average grain sizes and the largest grain sizes were both taken as the characteristic parameters of the as-annealed microstructure. The results pointed out the importance of choosing an appropriate combination of annealing temperature and time in order to retain second-phase particles during annealing not only for preventing unrestricted grain growth but also for avoiding grain size inhomogeneity.

* Corresponding author.
E-mail address: aeivani@iust.ac.ir (A.R. Eivani).

https://doi.org/10.1016/j.jmrt.2021.09.049

1. Introduction

Magnesium and its alloys have shown great potential for structural applications in ground transport, aerospace and medical devices, thanks to their unique characteristics, most notably superior strength to density ratio, excellent dimensional stability, high impact and dent resistance, exceptional damping capacity, nontoxicity and biocompatibility [1]. However, due to the hexagonal close-packed (HCP) crystal structure of magnesium and thus limited independent slip systems at room temperature, magnesium and its alloys exhibit poor cold workability [2]. Therefore, metal-forming operations, such as extrusion and rolling, are usually carried out at elevated temperatures where the deformation of Mg alloys can be facilitated by the activation of twining, enhanced activity of basal slip, and slip/twin interactions [1–5]. The activation of twining is of particular importance in enhancing the formability of Mg alloys at elevated temperatures, and its extent is directly affected by temperature, strain rate and grain size [6–8].

During thermomechanical processing (TMP) of magnesium alloys, such as multi-pass rolling at a moderately elevated temperature, dynamic recrystallization usually occurs to a great extent, depending on the temperature, the number of passes and reduction ratio applied, often leading to a heterogeneously recrystallized microstructure. While strength is usually improved due to grain refinement and basal texture hardening created during TMP, ductility is compromised as a result of the concentration of basal texture [9]. In order to achieve an equiaxed grain structure and regain ductility, hot-worked magnesium alloys are usually subjected to an annealing treatment [10]. During annealing, microstructural evolution events, such as static recovery, recrystallization, grain growth, and precipitation or dissolution of second-phase particles, occur, which greatly affects the resultant mechanical properties [11,12]. In the case of magnesium alloys with an HCP crystal structure, second-phase particles [12], pre-existing twinning and annealing twinning [13,14] are the key factors affecting the annealing kinetics and the resultant microstructure, particularly the limiting grain size, at which grain growth ceases at a given temperature. Retention of second-phase particles that can pin grain boundaries is important to prevent unrestricted grain growth and achieve an optimum balance between the resultant strength and ductility [14].

Among the methods commonly used to describe microstructural evolution occurring in metals, crystal plasticity and continuum mechanics-based modeling has been successfully applied. Such a modeling method has demonstrated its capabilities of providing numerical insights into the micro/meso scale events occurring during and after deformation [15]. Its main drawbacks, however, include the low resolution and low accuracy of the classic metal plasticity models in the calculation domains. To overcome these drawbacks, atomistic simulation methods have been developed in the last three decades for modeling complex microstructure changes [16]. The Monte Carlo (MC) simulation method, for example, has been introduced for modeling recrystallization, grain growth, abnormal grain growth and phase transformation. The fundamental concept of the MC simulation is based on the relative site change of grain boundaries, based on energy balance through a computational updating act, i.e., re-orientation attempts in every unit zone or cell. Many investigations using the MC approach have been carried out to study the grain growth kinetics and to predict final grain sizes, topology and particle-pinned grain growth during annealing [15–18]. In addition, dynamic recrystallization [19] and microstructural evolution of thin films [21] have been simulated by using the MC method as well. Similar modeling approaches, such as molecular dynamics (MD) [20] and cellular automata (CA) [21], have been developed as the other numerical techniques and used for the simulation of microstructure changes. Nevertheless, the MC method is still preferred, due to its computational flexibility and physical analogy to the physical phenomena involved in microstructure changes.

In this research, an attempt was made to take advantage of the capabilities of the MC method to predict the grain growth in the hot-rolled AZ61 Mg alloy, considering the presence of second-phase particles. The fraction of second-phase particles affecting grain growth was taken as a function of annealing time and temperature. It was hypothesized that the presence of second phase particles would affect the kinetics of grain growth and determine the resultant grain structure. Accordingly, second-phase particles were taken into consideration in establishing an accurate and reliable model for predicting the resultant grain structure of the AZ61 magnesium alloy. Comparisons were made with experimental data and those derived from an analytical model.

2. Mathematical models describing grain growth in the presence of second-phase particles

Considering the curvature of grain boundaries, the driving force of grain growth is expressed by Eq. (1):

$$P = \frac{\alpha \gamma_b}{R} \tag{1}$$

where R is the curvature radius of grain boundary, γ_b represents the grain boundary surface energy, and α is a geometry-related constant. In the presence of second-phase particles, the mobility of grain boundaries tends to reduce. This is due to the drag force exerted by particles, i.e., the Zener drag pressure P_z, which can be expressed as [12]:

$$P_z = \frac{3F_v \gamma_b}{2r} \tag{2}$$

where F_v and r are the volume fraction and radius of second-phase particles, respectively. Based on the energy balance concept, the mobility of grain boundaries in the presence of second-phase particles can be calculated as:

$$\frac{dR}{dt} = M(P - Pz) = M\left(\frac{\alpha \gamma_b}{R} - \frac{3F_v \gamma_b}{2r}\right) \tag{3}$$

where M is a constant expressing the mobility of grain boundaries, depending on the chemical composition and the

anisotropic characteristics of boundary zones. Considering the terms in Eq. (3), it can be inferred that the rate of grain growth is a parabolic function. However, it tends to decrease gradually towards zero with time, when $P=P_z$. This fact can be used as a stopping criterion in an iterative solution in the MC simulation by implementing Eq. (4):

$$\frac{dR}{dt}=0 \tag{4}$$

In another approach suggested by Hillert et al. [22], the influence of particle pinning on the kinetics of grain growth is taken into account by a slight modification of the growth rate of a single-phase material, based on Eq. (5):

$$\frac{dR}{dt}=c\gamma_b\left(\frac{1}{R_{crit}}-\frac{1}{R}\pm\frac{z}{c}\right) \tag{5}$$

where R_{crit} is the time-dependent critical grain size, c is a constant being equal to 0.5 for 2D models and to unity for 3D models, and $z = 3F_v/4r$. For the grains falling into $\frac{1}{R}\pm\frac{z}{c}$, the net pressure for grain boundary migration approaches zero and thus no grain growth happens. In the MC model, after a number of incremental time epochs, grains tend to become larger or smaller and the aforementioned specific value may vary.

It has been shown that the grain boundary pressure caused by particle pinning becomes equal to the driving pressure during grain growth. At such a time point, the grain growth driven by grain boundary migration ceases and a limiting grain size is reached [12]. In other words, grain growth stops, when $P=P_z$, and, therefore, by combining Eqs. (1) and (2), one can rewrite:

$$\frac{\alpha\gamma_b}{R}=\frac{3F_v\gamma_b}{2r} \tag{6}$$

Setting the value of α to one, the Zener limiting grain size can be estimated, using Eq. (7):

$$D_z=4r/3F_v \tag{7}$$

In another approach to describing grain growth, the degree of the contact between grain boundaries and second-phase particles is considered to predict the limiting grain size in the presence of second-phase particles. The degree of the contact increases during grain growth and reaches a stable value, when the grain structure is pinned [23]. In the novel geometrical computational model proposed by Gladman [24], the effect of particles on grain growth or shrinkage is considered, leading to Eq. (8):

$$D_z=\frac{\pi r}{3F_v}\left(\frac{3}{2}-\frac{2}{Z}\right) \tag{8}$$

where Z represents the ratio of the maximum grain size to the average grain size, a parameter which is not readily calculated, but it is expected to lie between 1.33 and 2. This model uses a set of similar cube-octahedral grains, of which one grain grows at the outlay of its neighbors. This model is a preliminary point for the explanation of abnormal grain growth. Although the dependence of D_z on F_v is successfully described, the accuracy of the proposed relationship for the material with a low volume fraction of second-phase particles is under question.

3. Monte Carlo simulation of grain growth and limiting grain size

In the present research, the Monte Carlo method was used to simulate the grain growth of the AZ61 magnesium alloy containing second-phase particles taken into account. First of all, the lattice as the main calculation domain was transmitted into small three-cornered units. To present different grains with unlike orientations, the initial microstructure was plotted in a field with 150 × 150 lattices. Every unit was quantified by an accidental number of S_i with i being between 1 and 64, representing its orientation. Residences with alike numbers were reflected to be one grain interior region, while grain boundaries were assumed to be the regions between two unlike neighboring lattices. The ultimate map illustrated a polycrystalline material consisting of grains with different orientations. This model was essentially an energy balance equation, as it was based on the grain boundary energy evolution during grain growth as a thermally activated process. At a given temperature, grain boundary migration occurred with time. Second-phase particles were assumed to have an unlike orientation, for example, $S_i = -1$. This was done to represent a realistic situation in the simulation of pinning pressure and its effect on grain boundary migration hindrance. The grain boundary energy was zero inside the grains and positive for the grain boundaries during energy updating algorithm. The iterative overall energy equation of the lattice used is as follows:

$$E_{GB}=\frac{J}{2}\sum_{i=1}^{M}\sum_{j=1}^{N}\left(1-\delta_{s_is_j}\right) \tag{9}$$

where J defines the grain boundary energy per unit length, M encompasses all the nearest neighbors of site i being 6 in this model, N is the total number of lattices in the system equal to 22,500 in this MC simulation, and $\delta_{s_is_j}$ is the Kronecker delta.

The time in the MC simulation was defined by the virtual time, which was Monte Carlo steps (MCSs). Each MCS in this simulation represented 22,500 (for a 150 × 150 lattice structure) reorientation attempts. MCS was assumed to be linearly correlated with the physical time using a jump frequency that depended on temperature. In order to compare the MC predictions with experimental results, the virtual MC simulation time was converted into real time (s) using Eq. (10):

$$1\,(MCS)=\frac{d^2}{6D_{GB}Q} \tag{10}$$

where D_{GB}, d and Q are the grain boundary diffusion coefficient, model lattice constant and number of orientations, respectively. In this research, the terms of d and Q had values of 1 and 64, respectively.

It should be noted that all the parameters involved in the above-mentioned equation were calculated from a lattice with at least 100 mapped grains in every direction of a 2D model. To

calculate D_{GB}, the Arrhenius-type mathematical description of diffusion coefficient was employed, based on Eq. (11):

$$D_{GB} = D_{0GB} \exp\left(\frac{-Q_{GB}}{RT}\right) \quad (11)$$

In which, R and T are the gas constant and absolute temperature, respectively. In order to scheme grain growth with relatively multifaceted nature of its involved metallurgy, a simplified perception based on conventional statistical procedure was applied. The grain boundary energy is related to the interaction energy between nearest neighbor sites. A grain boundary segment is defined to lie between two sites of unlike orientations. In the developed algorithm, if the energy variation for two neighboring lattice is less than zero, the new location can be accepted as the double situates will be reflected to be inside a new single grain. Or else, if the energy variation exceeds than zero, the fresh orientation can be deliberated based on Boltzmann probability function (Eq. (12)):

$$P = Exp(\Delta E / RT) = Exp(-S(n_2 - n_1) / BT) \quad (12)$$

where T is the absolute temperature, B is the Boltzmann constant, n_1 and n_2 is the number of orientations before after reorientation attempts, respectively. So, the average grain size can be computed based on the expression stated in Eq. (13):

$$L = (V/g)^{1/3} \quad (13)$$

where V is the volumetric calculation domain selected for MC simulation and g is the quantity of grains within the space V. To reflect the DRX occurrences through hot rolling, in every MCS, initial nucleates were arbitrarily distributed. It should be noted that the new orientation should be selected at random between all probable orientations while size distribution of pinned grains should be contracted than that of the pinning-free grains with the similar anisotropy of grain boundary energy. In order to simulate the consequence of precipitates on grain growth, the number of lattice points which corresponds to the amount of particles are designated at random and given a new number. Such sites are not permitted to change during re-orientation attempts. The particle/matrix interfacial energy is assumed to be the same as the matrix grain boundary energy. The effect of the number of particles on the average grain size was simulated in the following two cases: one is that particles do not travel or even coarsen and the other is that the number of particle may reduce with increase of simulation time [25].

4. Materials and experimental details

Round extruded bars of the AZ61 magnesium alloy with a diameter of 48 mm were used as the starting material in this investigation. The chemical composition of the alloy is given in Table 1. The rods were cut into rectangular plates with a length of 45 mm, width of 25 mm and thickness of 10 mm by using electro-discharge machine (EDM). The plates were subjected to a homogenization heat treatment at 400 °C for 5 h, followed by cooling in air. The homogenized plates, after being heated at 430 °C for 30 min, were hot-rolled at 430 °C and at a roller speed of 10 rpm for five passes to achieve a 55% reduction in thickness, followed by water quenching. The as-hot-rolled plates were then annealed at temperatures of 200, 300, 400 and 430 °C for 10, 20, 60, 300 and 600 min.

To reveal the microstructures of the as-hot-rolled and as-annealed samples, the Picral etchant was used for etching the samples, after grinding and subsequent polishing with 0.3 μm alumina powder. A statistical method according to ASTM E112 was used for determining the average grain sizes of all the samples annealed at different conditions.

Table 1 – The Chemical composition of AZ61 alloy used in this investigation.

Element	Mg	Al	Zn	Mn	Si	Cu	Fe
Wt. (%)	Balance	5.94	0.94	0.37	0.034	0.003	0.002

5. Results and discussion

5.1. *The as-homogenized and as-hot-rolled microstructures*

The initial microstructure of the alloy after homogenization at 400 °C for 5 h is shown in Fig. 1a. The microstructure was

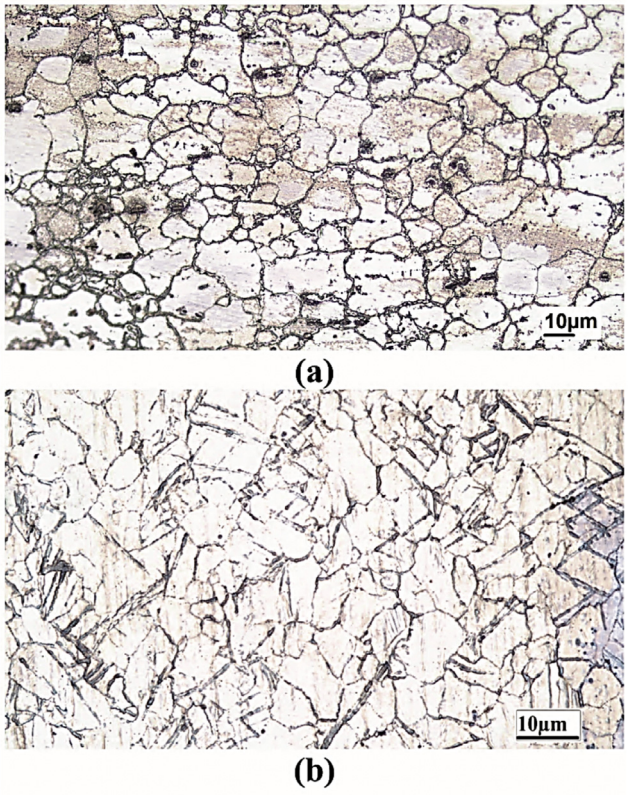

Fig. 1 – (a) The initial microstructure of the alloy after homogenization at 400 °C for 5 h and (b) the microstructure of the alloy after hot rolling at 430 °C.

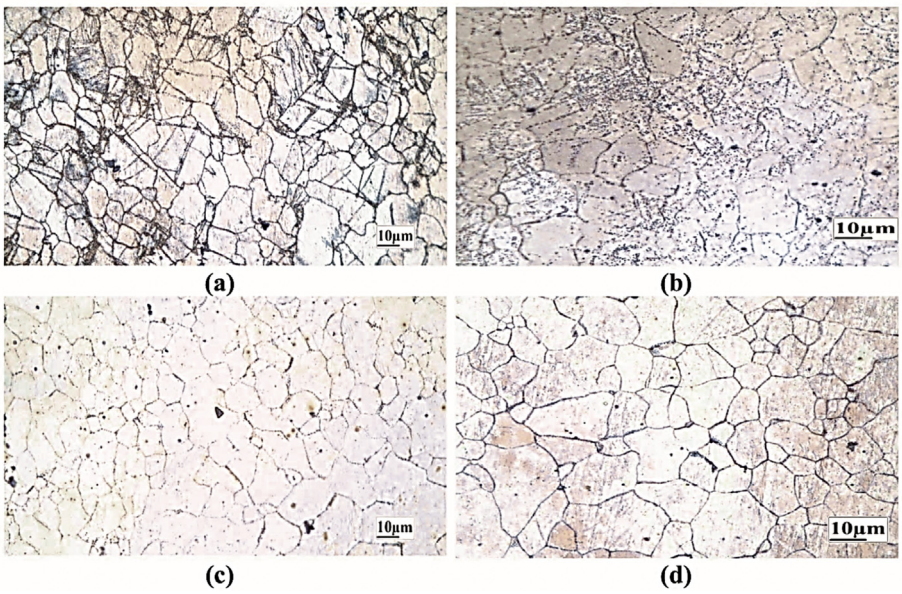

Fig. 2 – Microstructures of the samples after hot rolling at 430 °C, followed by annealing at (a) 200, (b) 300, (c) 400 and (d) 430 °C for 20 min.

composed of fully recrystallized fine, equiaxed grains with an average size of 20 μm and β-$Mg_{17}Al_{12}$ s-phase particles. No traces of twining which could have been introduced during extrusion could be observed.

The microstructure of the material after rolling at 430 °C is shown in Fig. 1b. Twinning was perceived in the form of parallel lines inside the deformed grains. No elongated grains were present and the average grain size was reduced to 10 μm, indicative of the occurrence of full dynamic recrystallization (DRX).

Through the initial stages of hot rolling, static recovery (SRV) advances recrystallization nuclei as fine dislocation-free zones as then, the expansion of recrystallization nuclei development is taking place. In this step, the recrystallization nuclei as fine dislocation-free crystallites tend to grow by the migration of the grain boundaries, which put the energy of strain-hardened microstructure away. Such nuclei are defined by low angle boundaries (LAGBs), the misorientation, of which gradually increase up to then that they reach to threshold values of high angle boundaries (HAB). During hot rolling of low SFE Mg alloy, the microstructure is a combination of recrystallized and strain hardened unrecrystallized grains known as discontinuous dynamic recrystallization (DDRX). Together with, the sub-boundary misorientation increases progressively till all the LAGBs are converted to HAB, and this type of microstructure remains homogeneous all over process. This restoration phenomenon tends to happens in strain hardened metals deformed at temperatures beyond half of their melting point. During hot rolling processes, the material is heated up before the process, and after during deformation, it stands simultaneous strain hardening and thermally-activated restoration phenomena [26]. According to the deformation processing map developed for AZ61 [27], at the rolling temperature of 430 °C, DRX is likely to proceed to completion, followed by grain growth. Almost no second-phase particles were observable, due to the quenching applied at the end of hot rolling.

5.2. *Effects of annealing parameters on the kinetics of grain growth*

The microstructures of the samples after annealing at 200, 300, 400 and 430 °C for 20 min are shown in Fig. 2. In the sample annealed at 200 °C (Fig. 2a), annealing twins appeared due to the partial coherent nature of twin boundary [28], apart from the pre-existing twins introduced during hot rolling. In addition, second-phase particles, i.e., β-phase particles, were observed. In the sample annealed at 300 °C, the precipitation of a larger fraction of second-phase particles occurred. These particles were expected to pin grain boundaries and inhibit grain boundary migration. Consequently, these second-phase particles could significantly affect the kinetics of grain growth. In the samples annealed at higher temperatures, i.e., 400 and 430 °C, however, second-phase particles appeared to be nearly not observable, obviously as a result of their dissolution in the α-Mg matrix. This would suggest that the rate of grain growth would sharply increase, due to the absence of the inhibiting effect of particles in addition to increased mobility of grain boundaries at a higher annealing temperature. In other words, the limiting grain size, being directly affected by the fraction of second-phase particles, would be significantly affected by annealing temperature. Annealing at a sufficiently high temperature could enable the Oswald ripening mechanism to operate, with which larger grains would grow further at the expense of smaller grains. Considering the dependence of grain boundary mobility on temperature, the rate-limiting factors are diffusion-controlled. Therefore, grain growth would occur exponentially faster with rising temperature, while varying linearly with increasing time at a given temperature. At a given temperature and at the beginning of

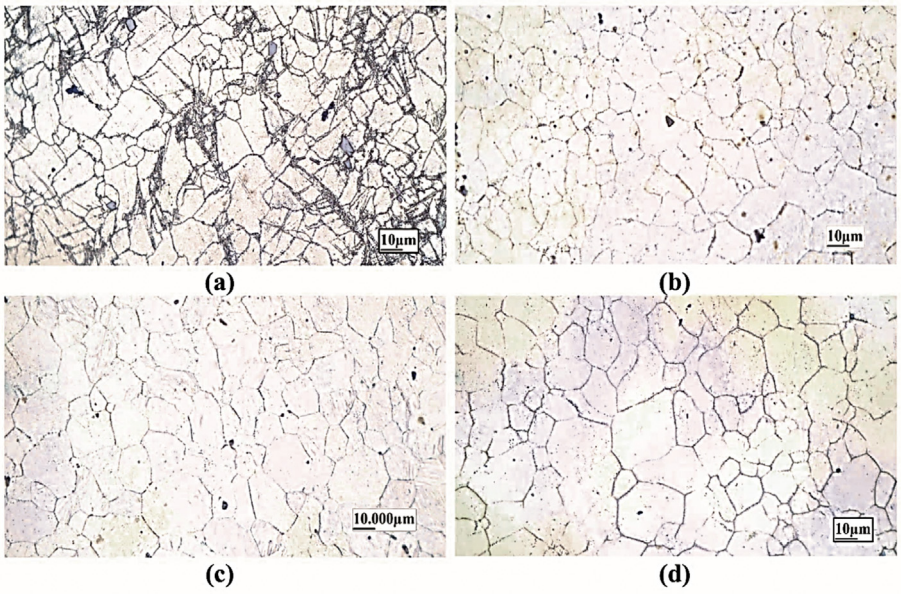

Fig. 3 – Effect of annealing time at 400 °C for (a) 10, (b) 20, (c) 300 and (d) 600 min on the microstructure of the samples hot-rolled at 430 °C.

annealing, grains sizes vary from very small ones to very large ones. The smallest grains having the largest surface area to volume ratio would be more likely to disband and shrink, resulting in the further growth of larger grains. This process is strongly promoted at an increased annealing temperature.

The evolution of microstructure as a function of annealing time in the samples rolled at 430 °C, followed by annealing at 400 °C, is presented in Fig. 3. It can be seen in Fig. 3a that after 10 min, fine recrystallized grains with twins were present, which were most likely the ones formed at the hot-rolling step. With an increase in annealing time to 20 min, however, these twins were eliminated and the sizes of grains remained largely unchanged (~10 μm). With an extension of holding time to 300 min, grain growth occurred and the average grain size became 17 μm. With a further increase in annealing time to 600 min, the average grain size remained at a value of 17 μm and thus the limiting grain size during annealing at 400 °C was reached. It is important to note that at this annealing temperature, the major part of second-phase particles appeared to be dissolved.

In addition to the grain structure, the volume fraction of second-phase particles changed during post-forming annealing. At different annealing temperatures, there were equilibrium volume fractions of precipitated second-phase particles, which could affect grain growth and thus the limiting grain size. It was therefore of interest to examine the second-phase particles in the material after annealing. Fig. 4 shows the microstructures of the samples annealed at temperatures of 200, 300, 400 and 430 °C for 600 min. To investigate the pinning effect of particles on the kinetics of grain growth, the fraction of second-phase particles at each annealing temperature was determined. All micrographs were exported to the Image-J image analysis software and the fraction of second phases was determined, which was subsequently implemented in the MC simulation. The fractions of second-phase particles were estimated to be 15%, 10%, 8% and 2% in the microstructures of the samples annealed at 200, 300, 400 and 430 °C, respectively. Corresponding to decreasing volume fraction of second-phase particles, the rate of grain growth increased, resulting in a larger limiting grain size at a higher annealing temperature. It can be seen in Fig. 4d that at 430 °C, grain sizes considerably increased due to a very low fraction of second-phase particles. In addition to the volume fraction, the sizes of second-phase particles could influence grain growth as well. Over the annealing temperature range applied in this research, the sizes of second-phase particles were however found to be unchanged, according to the data processed by Image-J. At 200 and 300 °C (Fig. 4a and b, respectively), the grain structures remained relatively fine and grain boundary migration was hard due to the presence of a large fraction of fine particles. With a moderate increase in annealing temperature, grain sizes only slightly increased and then the driving force for further grain growth declined with time and even became too low to overcome the pinning pressure exerted by particles. It can be seen in Fig. 4c that after annealing at 400 °C for 300 min, the grain boundaries were not effectively pinned by second-phase particles any more. Therefore, the extent of grain boundary–particle interactions was smaller. During annealing at 430 °C for 300 min, considerable grain growth took place, as no effective pinning was imposed on grain boundaries (Fig. 4d). Consequently, grain boundary triple junctions are connected by straight lines and the morphology of grain boundaries becomes smoother in comparison to that in other samples.

5.3. *MC simulation of grain growth*

The microstructures predicted from the MC simulation with 150 × 150 lattices, $Q = 64$ and 1.5% second-phase particles ($T = 430$ °C) are shown in Fig. 5. After implementing the initial

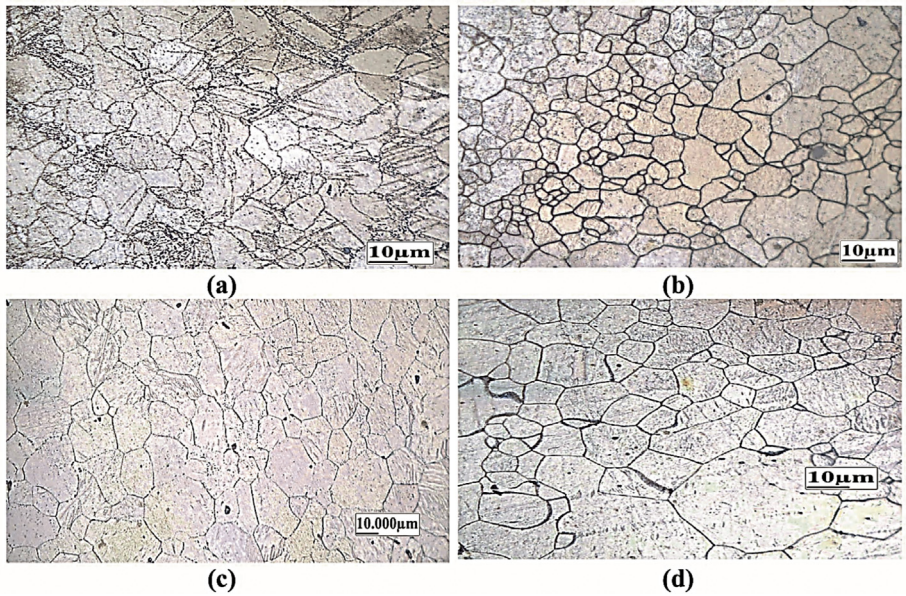

Fig. 4 – Microstructures of the samples after annealing at (a) 200, (b) 300, (c) 400 and (d) 430 °C for 300 min, containing 15%, 10%, 8% and 2% of second-phase particles, respectively.

microstructure into the model, it was observed that the onset of grain growth tended to commence at 260 MCSs and grain growth stopped at 15,000 MCSs when the limiting grain size was reached. It can be clearly seen that the microstructural evolution was directly affected by second-phase particles. At the onset of grain growth, governed by the power law, growth occurred in the regions free of second-phase particles. As the growth proceeded further, the grains with no particles at their boundaries experienced normal growth, while the boundaries pinned by second-phase particles could not move due to the pinning effect of particles. It is thus obvious that the MC simulation could effectively predict the pinning effect of second-phase particles, which inhibited grain boundary migration and grain growth.

The same MC simulation procedure was applied to predict the microstructures under other annealing conditions. Optical microscopy (OM) images of the microstructures of the hot-rolled AZ61 Mg alloy after post-forming annealing are

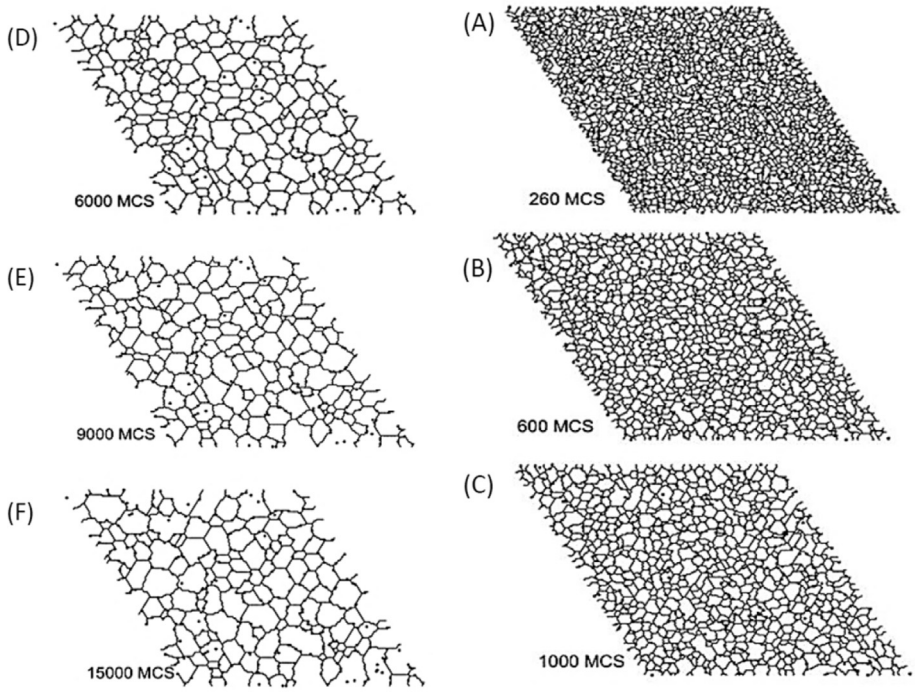

Fig. 5 – Monte Carlo prediction of the progressing as-annealed microstructure of AZ61 in the presence of 1.5% second-phase particles (indicated by black dots) at (a) 260, (b) 600, (c) 1,000, (d) 6,000, (e) 9,000, and (f) 15,000 MCSs.

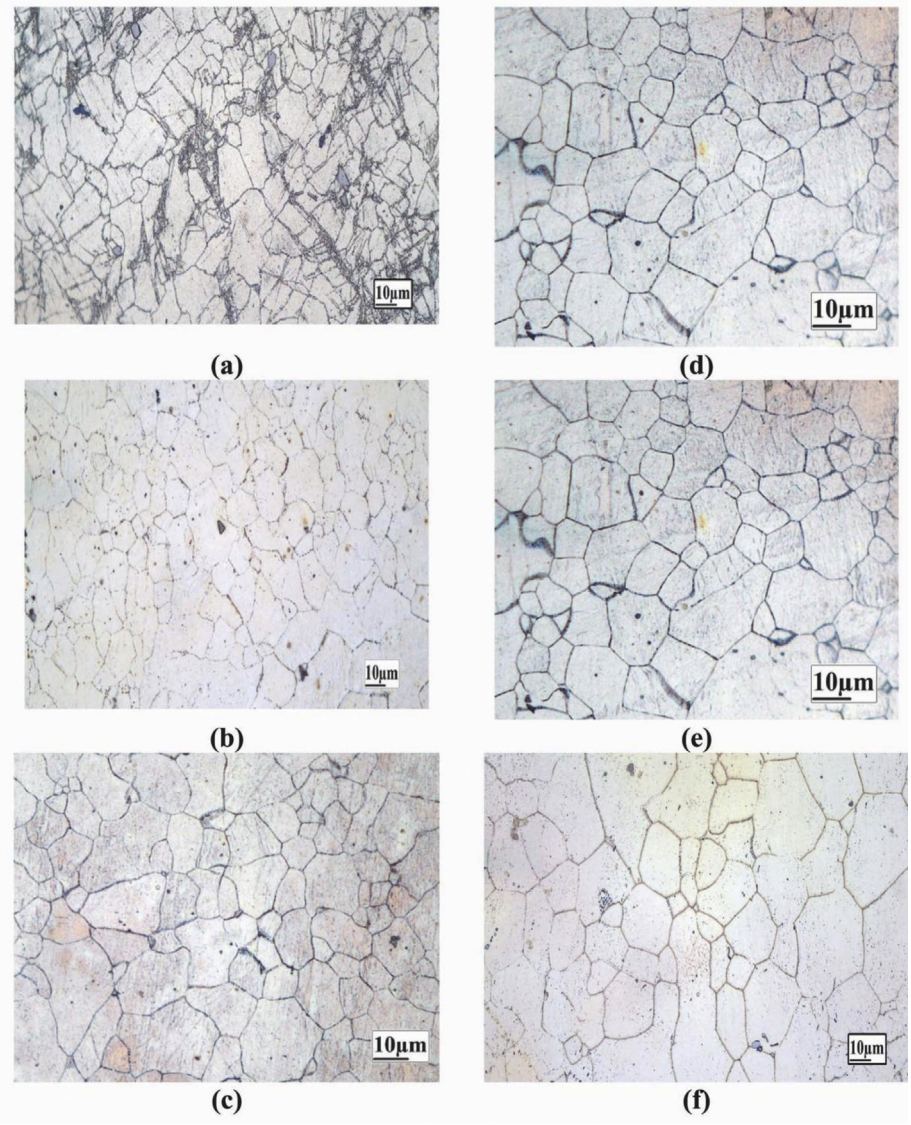

Fig. 6 – Optical microstructures of (a) the as-rolled material and the same material after annealing at 430 °C for (b) 10, (c) 20, (d) 60, (e) 300 and (f) 600 min.

presented in Fig. 6. It can be seen that the fraction of second-phase particles indeed decreased with increasing annealing time at 430 °C, leading to nearly complete dissolution of particles at 600 min. As a result, grain growth progressed to a large limiting grain size. At this time point, the geometrical morphology of grain boundaries would be determined by energy balance. This occurred at 15,000 MCSs during annealing at 430 °C. It could be inferred that a limiting grain size would be reached, when the energy equilibrium attained after the fraction of second phase particles remained unchanged with time. However, if the fraction of second-phase particles in the α-Mg matrix during annealing reduced due to a raised annealing temperature, the drag pressure would reduce and grain boundary migration would be promoted, leading to an enhanced rate of normal grain growth. Thus, the dominant mechanism was the grain boundary migration resulting from surface curvature, which was basically diffusion-controlled. Since the kinetics of grain growth was controlled by diffusion, which could be mathematically expressed by time and temperature, extended grain growth was observed in the samples held at a given annealing temperature for longer times. However, as mentioned earlier, at a given volume fraction of second-phase particles, the sensitivity of grain growth to temperature was more significant than that to holding time.

Fig. 7a and b displays the plots of the experimental and predicted normalized grain sizes against annealing time at different annealing temperatures. As can be clearly seen from both the experimental and simulation results, with a lower volume fraction of second-phase particles, e.g., in the sample annealed at 430 °C, grain growth occurred at a higher rate, leading to a coarser grain structure. With a larger fraction of second-phase particles at a lower annealing temperature, the limiting grain size reduced and attained at a shorter time. The Monte Carlo predictions showed that grain growth was fully inhibited at 15,000, 12,000, 9000 and 6000 MCSs with

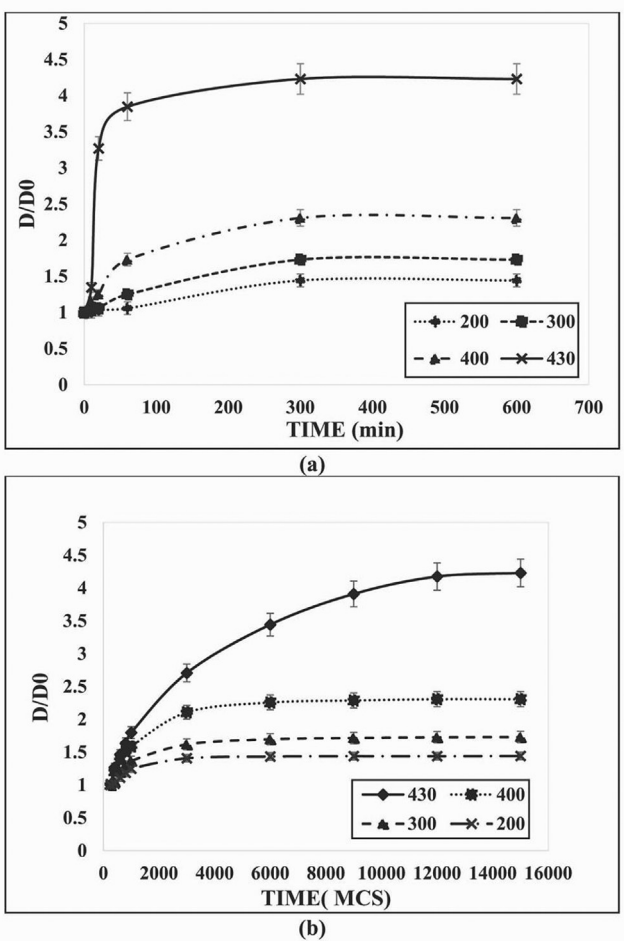

Fig. 7 – Plots of the normalized average grain sizes against annealing time, obtained from (a) experiments and (b) Monte Carlo simulation.

increasing fraction of second-phase particles from 1.5 to 8, 10 and 15%, respectively. Indeed, increasing the fraction of second-phase particles could significantly affect their pinning effect, as indicated by the reduced limiting grain sizes. As the fraction of second-phase particles decreased with annealing time, the average grain size increased, following the power law. Grain boundaries were relatively flat, when they were pinned by second-phase particles. Nevertheless, localized curvature in grain boundaries occurred, when these sections of grain boundaries intersected two or more particles. The results obtained from the MC simulation are in agreement with the observations of other researchers regarding grain growth kinetics [29–31].

It is important to note that small discrepancies between the MC predictions and experimental results did exist. Ignoring microstructure features, such as twining and the sizes and shape of second-phase particles, must have caused the discrepancies between the experimental and MC simulation results. Twining could be assumed to be a kind of low-mobility grain boundaries (i.e., Σ3 grain boundaries) [32], being able to prevent grain boundary migration. Consequently, the limiting grain size became smaller, when annealing temperature decreased to allow annealing twinning to occur. In addition, grain boundary energy and mobility were both missing in the mathematical expression of the Zener pinning effect, and therefore their effects on grain growth were not included in the MC simulation. Another source of discrepancies could be that in the simulation paradigm, second-phase particles were assumed to stay incoherent with the α-Mg matrix and spherical, whereas the $Mg_{17}Al_{12}$ precipitates in AZ61 were somehow semi-coherent and not fully spherical [33,34]. Moreover, abnormal grain growth caused by anisotropy in the mobility of grain boundaries was not taken into account in the MC simulation.

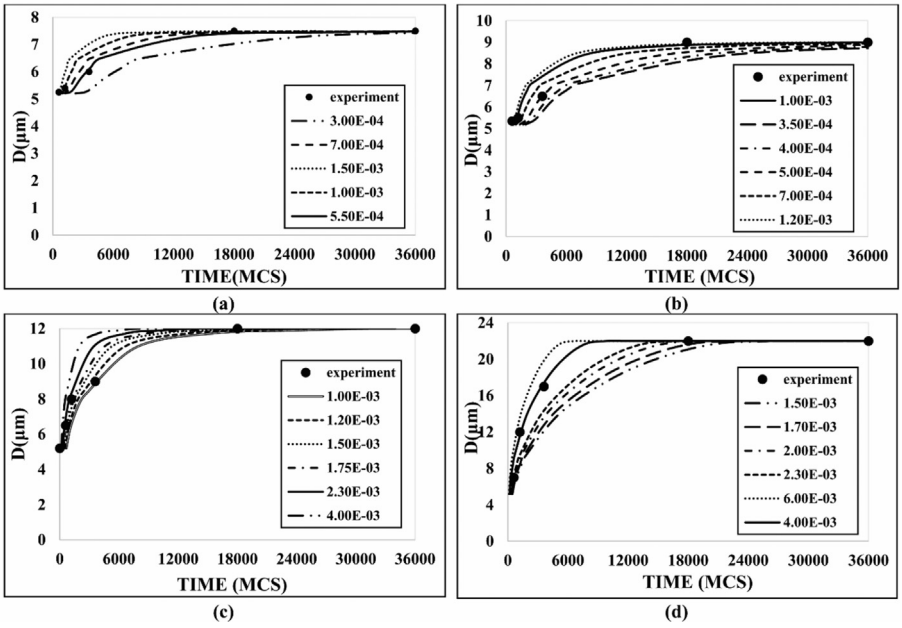

Fig. 8 – Assessment of experimental versus estimated data for the determination of D_{GB} for the AZ61 alloy at annealing temperatures of (a) 200, (b) 300, (c) 400, and (d) 430 °C.

Incorporation of these microstructural features are expected to improve the accuracy of the MC predictions significantly.

5.4. *Time conversion in the Monte Carlo simulation*

As mentioned earlier, the MC simulation was, in principal, carried out, based on the virtual time, called Monte Carlo steps (MCSs). Therefore, for a clear understanding of the growth kinetics and resultant grain sizes, MCS needed to be converted into real time, for example, through Eq. (10). In this equation, the value of grain boundary coefficient, D_{GB}, is the main parameter that had to be derived and implemented. Although the values of D_{GB} for some pure metals could be found in the literature, those for many commercial alloys are not available. In this case, one would have to determine the required data for a particular alloy. To do so, the least squares fitting was employed to calculate D_{GB} (Fig. 8) as a function of time at different annealing temperatures. Various D_{GB} values were then incorporated into the model to find the best correspondence between the experimental and predicted results.

Fig. 9 depicts the variation of D_{GB} with annealing temperature, corresponding to the fraction of second-phase particles, after linearization. The logarithmic form of Eq. (11) was employed to determine the activation energy Q and D_{0GB} by using Eq. (16):

$$\mathrm{Ln}\, D_{GB} = \mathrm{Ln}\, D_{0GB} - \frac{Q}{RT} \tag{14}$$

where the slope of the line in the logarithmic D_{0GB} versus 1/T plot was equal to −Q/RT. According to the fitting with a good correlation coefficient ($R^2 = 0.96$), the values of Q_{GB} and D_{0GB} were determined to be 22,167 J/mol and $1/41{,}9 \times \ 10^{-3}$, respectively.

In order to find the grain growth exponent *n*, Eq. (15) was used:

$$D^2 - D_0^2 = Ct^n \tag{15}$$

In Fig. 10, the best squares fitting method was employed to determine the *n* value in Eq. (15). The extracted data are listed in Table 2. It can be seen that with rising annealing temperature, the grain growth exponent *n* increased. Although the nature of grain boundaries did not change with the variation in temperature, the variations in the fraction of second-phase particles and thus their pinning effect on grain boundary migration resulted in the variation in the grain growth exponent. Because the grain growth exponent and grain boundary migration are mostly dictated by the diffusion-controlled mechanism, temperature plays a significant role in determining the grain growth exponent and grain boundary migration. The experimentally extracted value of the grain growth exponent did not reach a value close to 0.5, since there were a number of factors that could influence grain growth, including twining and the sizes and distribution of second-phase particles. It has been proposed that the twining activation region can be defined, when the slope of the curves equals zero. By raising annealing temperature, this region shrinks, indicating the reduction of twining activation. In other words, twinning activation percentage tends to rise, when annealing temperature decreases.

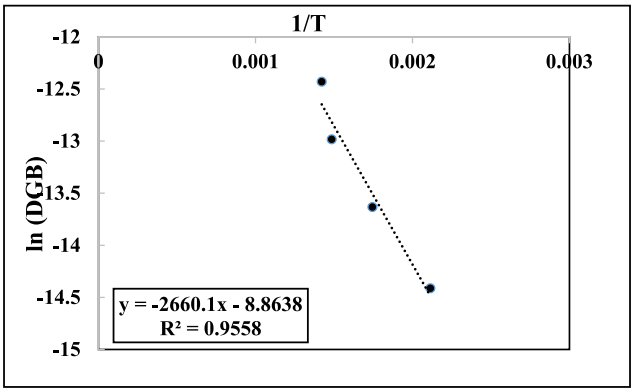

Fig. 9 – Variation of D_{GB} with reciprocal temperature.

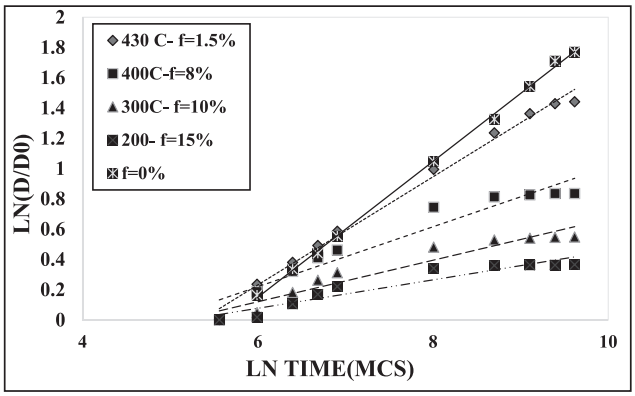

Fig. 10 – Variation of logarithmic normalized grain size with logarithmic time at different annealing temperatures.

The homogeneity of a grain structure can be evaluated by assessing the largest grain present at each of the annealing conditions, relative to the corresponding average grain size. When the ratio of the largest grain to the normal grain falls into a range of 2.5–3, it can be stated that the homogeneity of a grain structure is achieved and abnormal grain growth has not taken place [35]. The diameters of the largest grains of the AZ61 alloy with second-phase particles are shown in Fig. 11. It can be seen that with increasing fraction of second-phase particles (i.e., 0%, 1.5%, 8%, 10% and 15%), (150×150 and Q = 64), the largest grain size tended to decrease. Clearly, the most significant grain growth occurs when second-phase particles are absent, which is in full agreement with previous work [35]. The substantial difference in the largest grain size between the material with 0% and 1.5% second-phase particles indicates that the presence of second-phase particles, even of a small fraction, can still effectively affect grain

Table 2 – Grain growth exponent of the AZ61 Mg alloy at different temperatures.

(°C) Temperature	(*n*)grain growth exponent
200	0.094
300	0.14
400	0.2
430	0.36

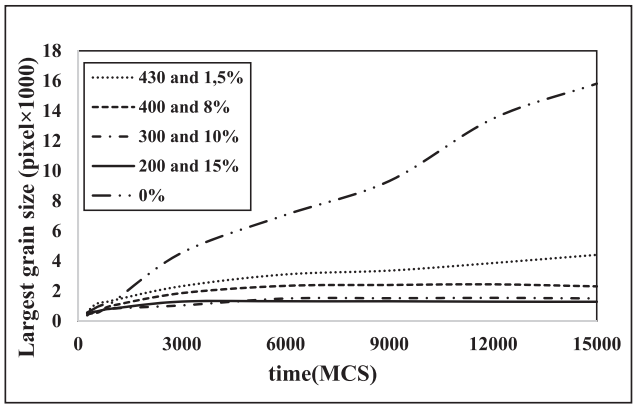

Fig. 11 – Variation of the largest grain size with time during annealing at different temperatures.

boundary migration by impeding grain boundaries and, consequently, the kinetics of normal grain growth. The aforementioned effect can be noticed in Fig. 12, which shows that a decrease in the largest grain size is achieved at a higher fraction of second-phase particles and that the largest grain size sharply increases with decreasing fraction of second-phase particles.

Thus, different levels of inhomogeneity in grain structure at different annealing temperatures can be clearly observed by comparing all the simulated microstructures with different fractions of second-phase particles in terms of the average grain size and the largest grain size, as the ratio can be used as an inhomogeneity index for rolled and annealed materials [36,37]. A decrease in the fraction of second-phase particles causes an enlarged difference between the sizes of the finest and largest grains. More uniform grain growth occurs through grain boundary migration at a higher fraction of second-phase particles. On the other hand, when the volume fraction of second-phase particles is low enough, the growth of the largest grain tends to occur at a rate similar to that of the smallest one. In short, a higher volume fraction of second-phase particles leads not only to smaller grain sizes but also to a more uniform grain size distribution.

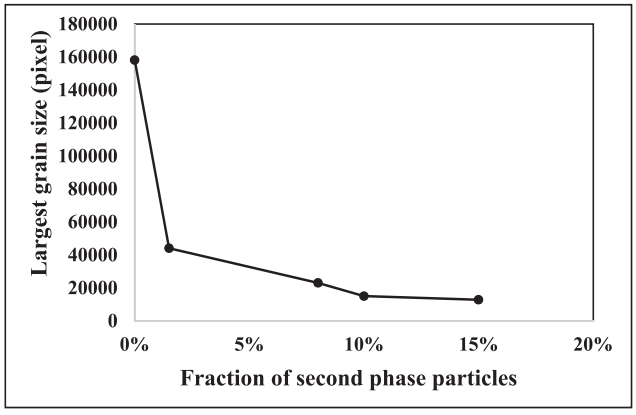

Fig. 12 – Variation of the largest grain size with the fraction of second-phase particles.

5.5. *Analytical model for grain growth*

In addition to the MC simulation, an additional effort was made to determine the kinetics of grain growth in the AZ61 magnesium alloy by means of an analytical model – an approach that was applied to predict grain growth during austenitization in low alloy steels [38,39]. According to the Sellars model [39], grain growth can be described by Eqs. (16) and (17):

$$d^n = d_0^n + Ate^{-Q/RT} \tag{16}$$

$$d = Bt^m e^{-Q/RT} \tag{17}$$

where d is the final grain size, d_0 the initial grain size (μm), T is temperature (K), t is time (min), R is the universal gas constant, and Q is the activation energy for grain growth (J/mol), while A, B, n, and m are the material constants that can be derived by calculations. To establish a comprehensive model for the prediction of grain size, Eq. (18) can be derived:

$$d^n = d_0^n + (At + Bt^m)e^{-Q/RT} \tag{18}$$

For magnesium alloys, the value of n is greater than 1.5, while the value of m is greater than unity. The initial grain size in this study was measured to be 10 μm, and the value of t ranged from 10 to 300 min. For calculating the values of n and m, Eq. (18) can be restated by Eq. (19) as the modified expression of grain growth in the hot-rolled AZ61 Mg alloy:

$$d^n = d_0^n + At^m e^{-Q/RT} \tag{19}$$

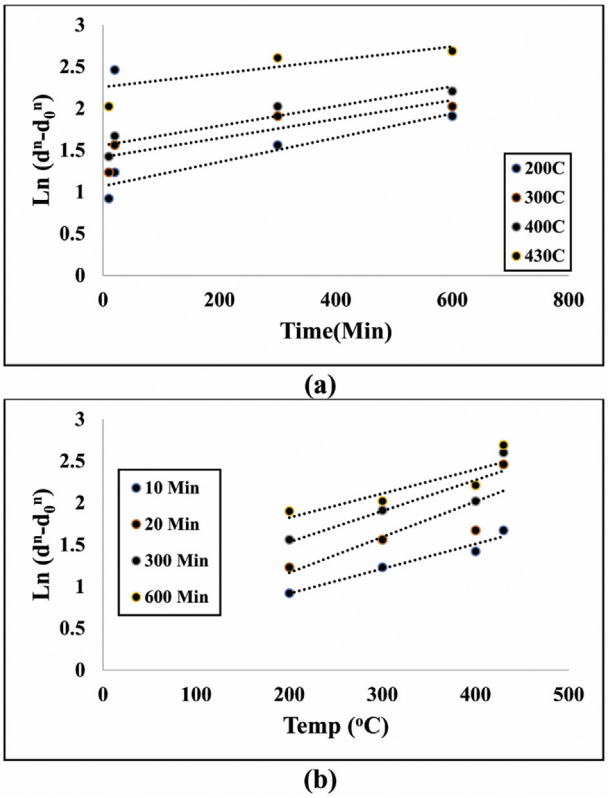

Fig. 13 – Variations of $ln\ln(d^n - d^n{}_0)$ with (a) annealing time and (b) annealing temperature.

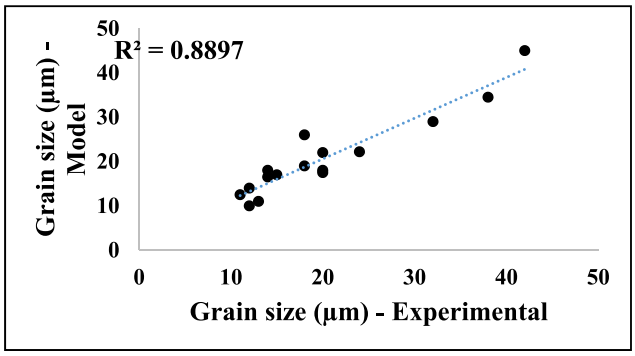

Fig. 14 – Cross-validation of the analytical model and experimental data.

where the values of A, Q, *n* and *m* cannot be determined by the linear regression method. In this case, an initial assumption of the *n* value was made and for the values of the other constants in Eq. (19), try and error calculations were performed. It was assumed that *n* varied over a range from 0.5 to 2, based on the data for Mg alloys. At a given time during annealing, Q could be obtained by using Eq. (20):

$$Q = -R \times \frac{\partial\left[lnln\left(d^n - d_0^n\right)\right]}{\partial\frac{1}{T}} = R \times S \tag{20}$$

According to the experimental data presented in Fig. 7a, by constructing $lnln\left(d^n - d^n{}_0\right)$ against 1/T plots, as shown in Fig. 13a, the slope of the curve representing the value of k could be determined. Then, Q could be determined and compared with the previously achieved values, according to Eq. (13), which was estimated to be 22,167 J/mol. After a round of try and error calculations, an appropriate *n* value was identified to be 1.312 for the AZ61 magnesium alloy over the mentioned temperature range. The plots of $lnln\left(d^n - d^n{}_0\right)$ against annealing temperature and time for the evaluation of Q and *m* are depicted in Fig. 13. At a given annealing temperature, according to Eq. (19), the *m* value could be obtained by Eq. (21):

$$m = \frac{\partial\left[lnln\left(d^n - d_0^n\right)\right]}{\partial lnln\, T} \tag{21}$$

According to the data presented in Fig. 13b and the fact that the slope of the curve is *m*, and using the determined values of *m*, *n* and Q, the value of A was calculated by using Eqs. (19)–(21). The values of m and A were determined to be 0.921 and 35,612, respectively. The linear correlation coefficient was 96%. Therefore, the grain growth model for the AZ61 alloy was expressed by Eq. (22):

$$d^{1.312} = d_0^{1.312} + 35612t^{0.921}e^{-22167/8.314T} \tag{22}$$

The comparison between the calculated results from the analytical model and experimental data is shown in Fig. 14.

Table 3 – Comparison of accuracy between the MC and analytical model predictions.

Approach	Assessment criteria	
	R^2	RMSE
Monte Carlo	96%	2.138
Analytical	93.5%	5.135

It can be seen that the model predictions were in good agreement with experimentally measured grain sizes. The comparisons between the predictions of MC simulation and analytical model against experimental data were done using criteria expressed by Eqs. (23) and (24), are shown in Table 3.

$$Root\ Mean\ Square\ Error = \sqrt{\frac{1}{N}\sum_{i=1}^{N}\left(d_i - p_i\right)^2} \tag{23}$$

$$Coefficient\ of\ determination\left(R^2\right) = 1 - \frac{\sum_{i=1}^{N}\left(d_i - p_i\right)^2}{\sum_{i=1}^{N}\left(d_i - d_{avg}\right)^2} \tag{24}$$

where d_i represents the desired (observed/measured/target) values, d_{avg} is the average of desired values, p_i is the predicted value, and p_{avg} is the average of the predicted values. It is clear that the MC simulation could predict the kinetics of grain growth with a higher accuracy.

6. Conclusions

Based on the results obtained in the present research, the following conclusions could be drawn.

1. A reasonable agreement between the experimental average grain sizes and the predicted values from the MC simulation was achieved. A higher accuracy could have been achieved when other microstructural features, such as twining, had been included in the MC simulation.
2. An increase in the fraction of second-phase particles led to a reduction in the size of the largest grain, in addition to a reduction in the average grain size. A reduction in the size of the largest grain, relative to the corresponding average grain size, indicates less microstructural inhomogeneity. Therefore, the microstructural homogeneity increases with increasing fraction of second-phase particles.
3. The growth rate of the largest grain became similar to that of the other grains when the pinning effect of second-phase particles on grain growth was absent, because the largest grain could form and grow as the other grains, virtually not inhibited by pinning particles.
4. The retention of second-phase particles was demonstrated to be an important factor for achieving a uniform grain size distribution and small grain sizes, due to the pinning effect on grain boundaries during annealing. The choice of annealing temperature and time should therefore be made with this factor in mind.
5. The comparisons of the calculated results from the MC and analytical models with the experimental data showed that the predicted data with the MC model was in better agreement with the experimental data.

Declaration of Competing Interest

The authors declare that they have no known competing financial interests or personal relationships that could have appeared to influence the work reported in this paper.

REFERENCES

[1] Luo A, Renaud J, Nakatsugawa I, Plourde J. Magnesium castings for automotive applications. J Occup Med 1995;47:28–31.
[2] Mordike B, Ebert T. Magnesium: properties—applications —potential. Mater Sci Eng, A 2001;302:37–45.
[3] Korla R, Chokshi AH. Strain-rate sensitivity and microstructural evolution in a Mg–Al–Zn alloy. Scripta Mater 2010;63:913–6.
[4] Jain A, Agnew SR. Modeling the temperature dependent effect of twinning on the behavior of magnesium alloy AZ31B sheet. Mater Sci Eng, A 2007;462:29–36.
[5] Song WQ, Beggs P, Easton M. Compressive strain-rate sensitivity of magnesium–aluminum die casting alloys. Mater Des 2009;30:642–8.
[6] Karimi E, Zarei-Hanzaki A, Pishbin M, Abedi H, Changizian P. Instantaneous strain rate sensitivity of wrought AZ31 magnesium alloy. Mater Des 2013;49:173–80.
[7] Yang X, Miura H, Sakai T. Dynamic evolution of new grains in magnesium alloy AZ31 during hot deformation. Mater Trans 2003;44:197–203.
[8] Beer A, Barnett M. Microstructural development during hot working of Mg-3Al-1Zn. Metall Mater Trans 2007;38:1856–67.
[9] Xin W, Chen W, Hu L, Wang G, Wang E. Microstructure refining and property improvement of ZK60 magnesium alloy by hot rolling. Trans Nonferrous Metals Soc China 2011;21:s242–6.
[10] Galiyev A, Kaibyshev R, Gottstein G. Correlation of plastic deformation and dynamic recrystallization in magnesium alloy ZK60. Acta Mater 2001;49:1199–207.
[11] Ion S, Humphreys F, White S. Dynamic recrystallisation and the development of microstructure during the high temperature deformation of magnesium. Acta Metall 1982;30:1909–19.
[12] Humphreys FJ, Hatherly M. Recrystallization and related annealing phenomena. Elsevier; 2012.
[13] Yu Z, Choo H. Influence of twinning on the grain refinement during high-temperature deformation in a magnesium alloy. Scripta Mater 2011;64:434–7.
[14] Liu Y, Wu X. A microstructure study on an AZ31 magnesium alloy tube after hot metal gas forming process. J Mater Eng Perform 2007;16:354–9.
[15] Anderson M, Srolovitz D, Grest G, Sahni P. Computer simulation of grain growth—I. Kinetics. Acta Metall 1984;32:783–91.
[16] Grest G, Srolovitz D, Anderson M. Computer simulation of grain growth—IV. Anisotropic grain boundary energies. Acta Metall 1985;33:509–20.
[17] Srolovitz D, Anderson MP, Sahni PS, Grest GS. Computer simulation of grain growth—II. Grain size distribution, topology, and local dynamics. Acta Metall 1984;32:793–802.
[18] Srolovitz D, Anderson M, Grest G, Sahni P. Computer simulation of grain growth-III. Influence of a particle dispersion. Acta Metall 1984;32:1429–38.
[19] Holm EA, Miodownik MA, Rollett AD. On abnormal subgrain growth and the origin of recrystallization nuclei. Acta Mater 2003;51:2701–16.
[20] Yamakov V, Wolf D, Phillpot S, Gleiter H. Grain-boundary diffusion creep in nanocrystalline palladium by molecular-dynamics simulation. Acta Mater 2002;50:61–73.
[21] Liu Y, Baudin T, Penelle R. Simulation of normal grain growth by cellular automata. Scripta Mater 1996;34.
[22] Hillert M. On the theory of normal and abnormal grain growth. Acta Metall 1965;13:227–38.
[23] Gao J, Thompson RG, Patterson BR. Computer simulation of grain growth with second phase particle pinning. Acta Mater 1997;45:3653–8.
[24] Gladman T. On the theory of the effect of precipitate particles on grain growth in metals. Proc Roy Soc Lond Math Phys Sci 1966;294:298–309.
[25] Khodabakhshi F, Aghajani Derazkola H, Gerlich AP. Monte Carlo simulation of grain refinement during friction stir processing. J Mater Sci 2020;55(27):13438–56.
[26] Aghajani Derazkola H, García Gil E, Murillo-Marrodán A, Méresse D. Review on dynamic recrystallization of martensitic stainless steels during hot deformation: Part I—experimental study. Metals 2021;11(4):572.
[27] Wu H-y, Wu C-t, Yang J-c, Lin M-j. Hot workability analysis of AZ61 Mg alloys with processing maps. Mater Sci Eng, A 2014;607:261–8.
[28] Sabat RK, Panda D, Sahoo SK. Growth mechanism of extension twin variants during annealing of pure magnesium: an 'ex situ' electron backscattered diffraction investigation. Mater Char 2017 Apr 1;126:10–6.
[29] Wu Y, Zong BY, Zhang XG, Wang MT. Grain growth in multiple scales of polycrystalline AZ31 magnesium alloy by phase-field simulation. Metall Mater Trans 2013;44(3):1599–610.
[30] Asadi P, Givi MKB, Akbari M. Simulation of dynamic recrystallization process during friction stir welding of AZ91 magnesium alloy. Int J Adv Manuf Technol 2016;83(1–4):301–11.
[31] Pozzo M, Alfe D. Structural properties and enthalpy of formation of magnesium hydride from quantum Monte Carlo calculations. Phys Rev B 2008;77(10):104103.
[32] Saito Y. The Monte Carlo simulation of microstructural evolution in metals. Mater Sci Eng, A 1997;223:114–24.
[33] Li L, Nam ND. Effect of yttrium on corrosion behavior of extruded AZ61 Mg alloy. J Magnes Alloys 2016 Mar 1;4(1):44–51.
[34] Kim B, Kang B, Park Y, Park I. Influence of Pd addition on the creep behavior of AZ61 magnesium alloy. Mater Sci Eng, A 2011;528(18):5747–53.
[35] Olgaard DL, Evans B. Effect of second-phase particles on grain growth in calcite. J Am Ceram Soc 1986;69(11):272. C–.
[36] Haghighat SH, Taheri AK. Investigation of limiting grain size and microstructure homogeneity in the presence of second phase particles using the Monte Carlo method. J Mater Process Technol 2008;195:195–203.
[37] Vafaeenezhad H, Seyedein S, Aboutalebi M, Eivani A. Hybrid Monte Carlo–Finite element simulation of microstructural evolution during annealing of severely deformed Sn-5Sb alloy. Comput Mater Sci 2019;163:196–208.
[38] Lazar EA, Mason JK, MacPherson RD, Srolovitz DJ. A more accurate three-dimensional grain growth algorithm. Acta Mater 2011;59:6837–47.
[39] Sellars C, Whiteman J. Recrystallization and grain growth in hot rolling. Met Sci 1979;13:187–94.